Variability Analysis of Significant Wave Heights and Wind Waves in Riau Archipelago Sea part ALKI 1

Gandhi Napitupulu[1], Ayi Tarya[2*], I Gede Merta Yoga Pratama[1], Ignatius Sonny Winardhie[3]

1. Department of Earth Sciences, Faculty of Earth Sciences and Technology, Institut Teknologi Bandung, Bandung, 40132, Indonesia
2. Oceanography Research Group, Faculty of Earth Sciences and Technology, Institut Teknologi Bandung, Bandung, 40116, Indonesia
3. Exploration and Engineering Seismology Research Group, Faculty of Mining and Petroleum Engineering, Institut Teknologi Bandung, Bandung, 40132, Indonesia

*e-mail: ayi.tarya@itb.ac.id

ABSTRACT

The Riau Archipelago Sea is part of the Indonesian Archipelago Sea Lane (ALKI) 1, with a very high intensity of crossing ships. Analysis of surface wind speed and significant wave height is the most important for the safety and performance of offshore shipping. This research aims to study wave characteristics and wind speed by identifying the main factors that affect significant wave height and surface wind speed. Dominant factors that affect significant wave height and wind speed are needed to decide on the safest path and the best time before crossing in ALKI-1. Temporal and spatial analysis of the seasonal variability of significant wave height and wind speed using ECMWF data for 18 years. The data used are significant wave height data and wind speed every 6 hours during the period 2000 – 2018. Three observation points are used for temporal analysis, it is found that significant wave height and wind speed are influenced by two main factors, namely MJO and Monsoon. Maximum significant wave height and wind speed that occurs in the SON period for points 3 and the DJF period at points 1 and 2. MJO affects directly from phases one to eight for observation points 1, 2, and 3. The 4, 7, and 8 MJO phases affect the value of wave height and wave speed significantly, and the 1, 2, and 5 MJO phases affect wave height and wind speed weakly.

Keywords: ALKI 1, MJO, MJO phase, Monsoon, Significant wave height, Wind speed.

INTRODUCTION

Indonesia is the largest archipelagic country in the world consisting of five large islands and thousands of small islands of various shapes and sizes, and overall 70% of Indonesia's territorial area is the ocean. (Kusumastanto, 2021). The daily life of the Indonesian population is closely related to the sea. The territory of Indonesia is also located between the continents of Asia and Australia and is flanked by the Indian and Pacific Oceans (Listiyono *et al*., 2021). This condition makes Indonesia's sea areas have a very strategic position in international shipping routes for the benefit of the world economy (Harris *et al.*, 2021).

Riau Archipelago is a province in Indonesia, which consists of islands, with a total of 2,408 large and small islands. Its area is 252,601 km², about 95% is the ocean, and only about 5% is land (Syafril and Sujarwanto, 2015). According to the 2019 Shipping Statistics data, the Riau Archipelago is one of Indonesia's territories in the Indonesian Archipelago Sea Lane (ALKI) 1, which has the most ships traversed, reaching 7,292,302 tons (Fatimah, 2019). The high number of voyages must be supported by information and anticipation of changes in oceanographic conditions, especially the height of sea waves (Saputra *et al.*, 2020).

Waves are important in marine meteorological services (WMO, 2001; Siregar *et al.*, 2019). The frequent occurrence of high waves can certainly disrupt fishing activities (Marelsa and Oktaviandra, 2019), sea transportation between islands that can have an impact on people's lives on lands (Rozi *et al.*, 2021), such as the scarcity of food on several small islands and the disruption of

various development activities due to the obstruction of the supply of construction materials. Knowledge of the characteristics of significant wave heights (SWH) and wind speed are the most important physical oceanographic parameters for planning, sea voyages (Kurniawan and Khotimah, 2016), development and construction of infrastructure at sea such as ports, protection of coastal forms (Hadi and Sugianto, 2012). So further research is needed on wind speed and SWH that is temporally and spatially significant.

Temporal data analysis such as Empirical Mode Decomposition (EMD), S-Transform, Generalized S-Transform (GST), and Data Filtering. Spatial data analysis is also important considering that data on significant wave heights and wind speed are often taken through satellite image data. Generally, this data has a low resolution where which can cause data gaps at certain points. To overcome this, spatial data analysis using Ordinary Kriging (OK) can be used as an alternative to producing data interpolation (Usman *et al.*, 2022).

MATERIALS AND METHODS

Research Area

The location of this research is in the Indonesian Ship Route (ALKI) 1 as shown in Figure 1 which passes through the Riau Islands. Three observation points in different areas, namely Point 1 (105ºEL; 0.25ºNL), Point 2 (106º EL; 4.5ºNL), Point 3 (98.5ºEL; 5.25ºNL).

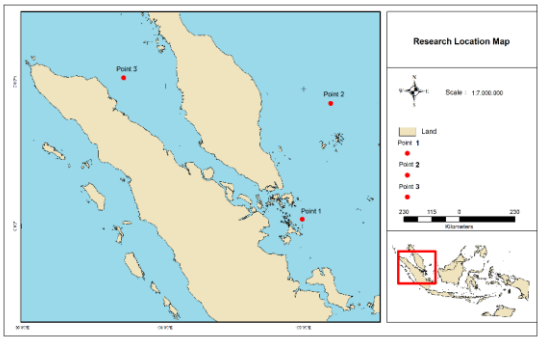

Figure 1. The research area of wave height variability in the Riau Archipelago

Data

Data used in this study are significant wave heights and wind speeds from 2000-2018 with an interval of every six hours. These data are model data with a resolution of 0.125^0 x 0.125^0 obtained from a reanalysis of interim-era datasets on the ECMWF page. (www.ecmwf.int/).

Reanalysis data is the result of a combination of field observation data with the output data of the prediction model at a location which is then combined into one value (Wang *et al.*, 2022). The spatial scale in reanalyzed data concerns a value that represents the extent of the data.

Empirical Mode Decomposition (EMD)

Empirical Mode Decomposition (EMD) is a time series data analysis technique developed as a basic part of the Hilbert-Huang Transform (HHT) (Zeiler *et al*., 2013). This EMD method separates high-frequency oscillation patterns of time series data from low frequencies and their trends using local temporal and empirical data characteristic structures (Sahoo *et al*., 2020).

The EMD algorithm can identify signal oscillations at the local level quickly and then the data is parsed through a process called shifting to form Intrinsic Mode Functions (IMF) which represent a single oscillatory portion of the signal that decomposes with amplitude and frequency that varies over time (Zeiler *et al*., 2013). All signals are parsed in the time domain and are of the same length as the original signal making it possible to maintain a frequency that varies in time (Huang *et al*., 2021).

S-Transform

S-Transform is a Time-Frequency Representation (TFR) or spectrum analysis that combines Wavelet Transform (WT) elements and Short Time Fourier Transform (STFT). This method is used to measure/represent the time-frequency of a time series or non-stationary signal (Lokhande *et al.*, 2017). The advantage of S-Transform is that the spectrum localization technique combines elements

from Wavelet Transform (WT) and Short Time Fourier Transform (STFT). This method is a generalization of the Gabor transform in which the width of the Gaussian window is scaled inversely and the window height is linearly scaled with frequency (Khetarpal and Tripathi, 2020).

Frequency Domain Filtering (FDR)

Frequency Domain Filtering (FDR) is used to remove unwanted signal parts such as random noise or extract used signal parts such as components that are within a certain frequency (Kolawole *et al.*, 2015). The advantage of using this filter according to the initial definition is that it can separate the desired signal components and does not change the original time series (Juan and Valdecantos, 2022).

Kriging (Ordinary Kriging - OK)

Kriging is a geostatistical data analysis method that is used to estimate the magnitude of the value that represents an unsampled point based on the sampled points around it using a semivariogram structural model. The OK method consists of ordinary point kriging and ordinary block kriging, where the prediction results with ordinary point kriging are in the form of points, while the prediction results for ordinary block kriging are in the area around the interpolation point. The OK method is the simplest kriging method found in geostatistics. In this method, the assumption is that the mean is unknown and constant, while the variogram is known. This method is a method that provides the Best Linear Unbiased Estimator-BLUE estimator (Bahtiyar *et al*., 2014).

RESULTS AND DISCUSSION

Empirical Mode Decomposition (EMD) Analysis

Empirical Mode Decomposition (EMD) method is used to obtain information in the form of Intrinsic Mode Function (IMF) from a complex data series signal. Figure 2 is the EMD result of the wind speed at point 1, and at points 2 and 3 (figure not shown) yields 10 IMF and residuals. IMF 1,2,3, and 4 contain signals with high frequencies, while IMF 5 to 10 contain signals with low frequencies. IMF 1 is a signal that has the lowest period or a signal with the highest frequency, then the frequency decreases as the order of the IMF increases. Fast Fourier Transform (FFT) is applied to all IMF EMD results to determine the periodicity of each IMF signal.

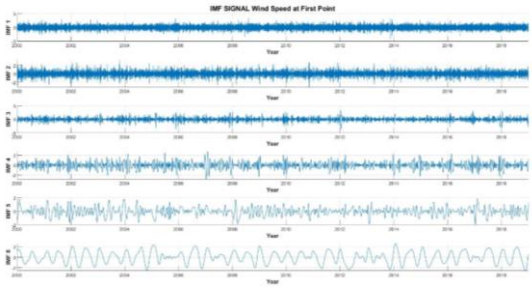

Figure 2. IMF results in 1 to 4 for wind speed at the first point.

The results of each IMF of wind speed and significant height were performed by FFT to see the data signal in the frequency domain as shown in Figure 3.

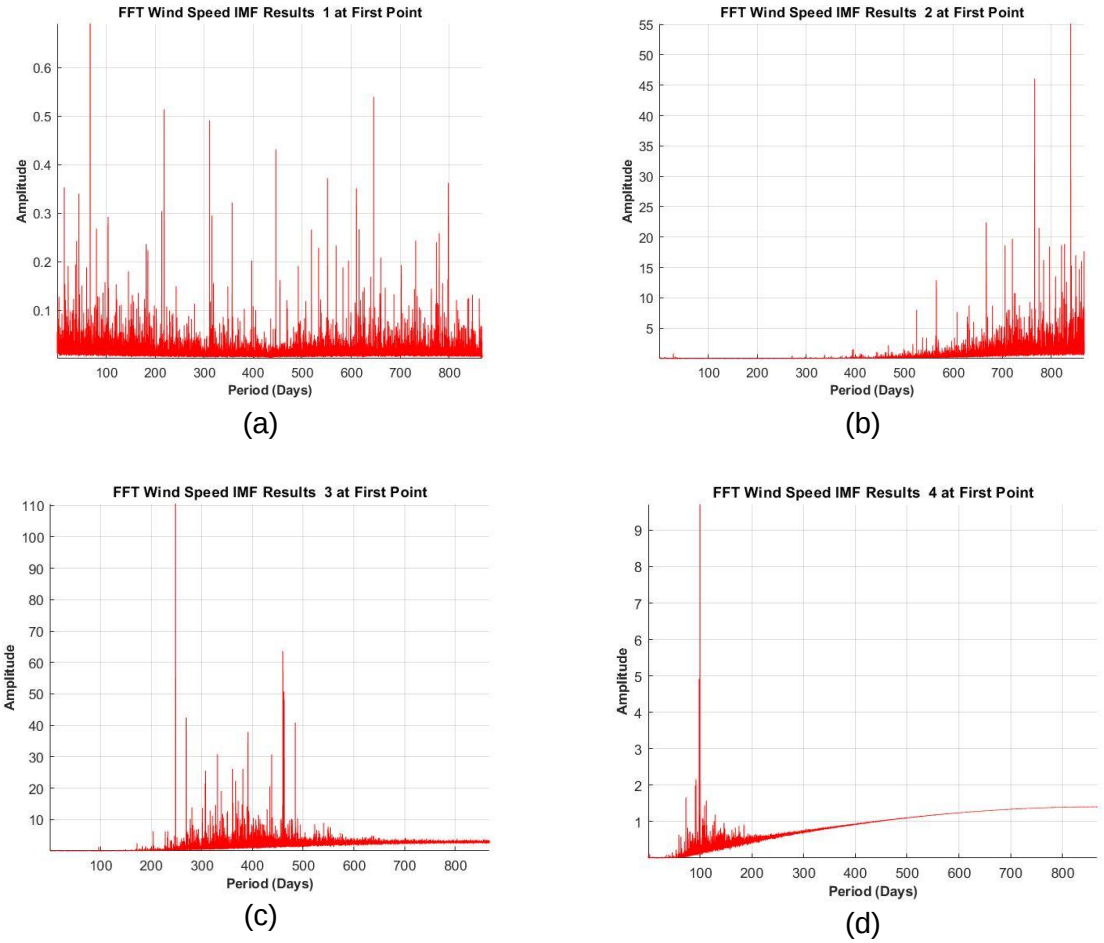

Figure 3. FFT of IMF results 1 (a), 2 (b), 3 (c), and 4 (d) at point 1 for wind speed

Figure 3 is the FFT periodogram of the wind speed and significant wave height of each IMF EMD result for points 1, 2, and 3 (figure not shown). The figure shows the existence of several dominant periods that have large amplitudes. Amplitude shows how strong it is when a certain period appears. The amplitude is the energy contribution to the period. It was found that the IMF 1 main periodicity component with a period of 67 days was in the Madden Julian Oscillation (MJO) phenomenon with a periodicity of 1-3 months (Madden and Julian, 1972). Furthermore, IMF 2 has a periodicity of 162 days in the 6 to 12-month periodicity range. IMF 3 is a signal with a periodicity of 6 months to 12 months within the range of the Monsoon phenomenon (Aldrian and Susanto, 2003). IMF 4 has a period of 100 days. IMF 5, IMF 6, IMF 7, IMF 8, IMF 9, and IMF 10 are not included in the discussion of this study because they have very long periodicity with low amplitude and the IMF signal does not correspond to atmospheric phenomena.

The FFT results show that only IMF 1, IMF 2, IMF 3, and IMF 4 have high amplitudes, much higher than other IMFs. IMF 1 and 4 have a periodicity corresponding to the MJO and IMF 2 and 3 have a periodicity corresponding to the Monsoon. This shows that the wind speed at a height of 10m at point 1 is influenced by two main factors, namely MJO and Monsoon. The FFT results for points 2 and point 3 also produce periodicity that corresponds to point 1. So that we get two main components that regulate the variability of Wind Speed (U_{10} and V_{10}) from 2000 to 2018 namely MJO and Monsoon.

The FFT results at significant wave heights yielded the same results, two main components regulate the variability of the SWH from 2000 to 2018, namely MJO and Monsoon. The pattern generated for each IMF at each point of view for Wind Speed and Significant Wave Height is the same because these two phenomena have a phase relationship (described in S-

Transform) so events related to Wind Speed will correspond to Significant Wave Height as well. The EMD results show that the FFT of each IMF with MJO and Monsoon periodicity corresponds to each IMF.

S-Transform and Generalized S-Transform Analysis

Data analysis using FFT cannot describe frequency and time simultaneously. The FFT cannot display what frequency is dominant at a certain time but only the dominant frequency at all times for stationary signals. Therefore, time-frequency analysis is needed to complete the existing data analysis. Stockwell-Transform is a useful tool for analyzing frequency response over time.

The S-Transform method provides a time-frequency representation of significant wave signals and wind speeds in a one-day sample rate at three points observation traversed by Indonesian Archipelago Sea Channel (ALKI) 1 for the period 2000-2018 so that phenomena that affect the variability of wave height and speed can be analyzed. wind. Signals that have variations with time can be analyzed using S-Transform. Results of processing wind speed using the S-Transform are shown in Figure 4.

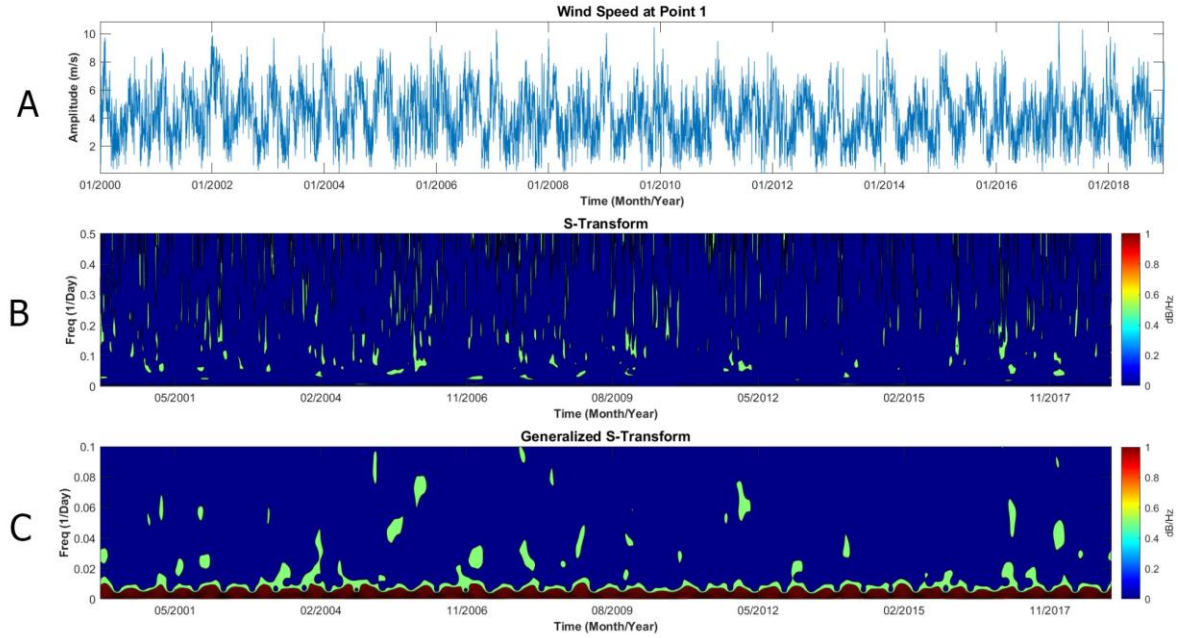

Figure 4. Time series data (A), S-Transform analysis (B) dan GST (C) analysis on wind speed at the first point

Figure 4A shows wind speed data from 2000 – 2018 with the x-axis representing time and the y-axis representing wind speed amplitude (m/s). Figure 4B is S-Transform results, showing a peak frequency that tends to be found in the middle of every year especially around June to July. Peak frequency value is 0.05/day - 0.15/day (15 - 20 days period). This low period indicates seasonal wind speed is influenced by local factors.

Further analysis will use the Generalized S-Transform (GST) as shown in Figure 4C. The results of the GST analysis pay attention to low frequencies. The GST result shows the value peak frequency is 0.01/day - 0.1/day (10 - 90 days period). This period shows a signal from the MJO phenomenon. The MJO is the dominant mode of intra-seasonal variability that affects climate and weather (Madden and Julian, 1994). When the MJO is active there is a significant increase in wind speed at an altitude of 1.5 km (Balbeid *et al*., 2015). This affects surface wind patterns (10 meters above sea level), which affects several parameters at sea (Jones *et al.*, 1998).

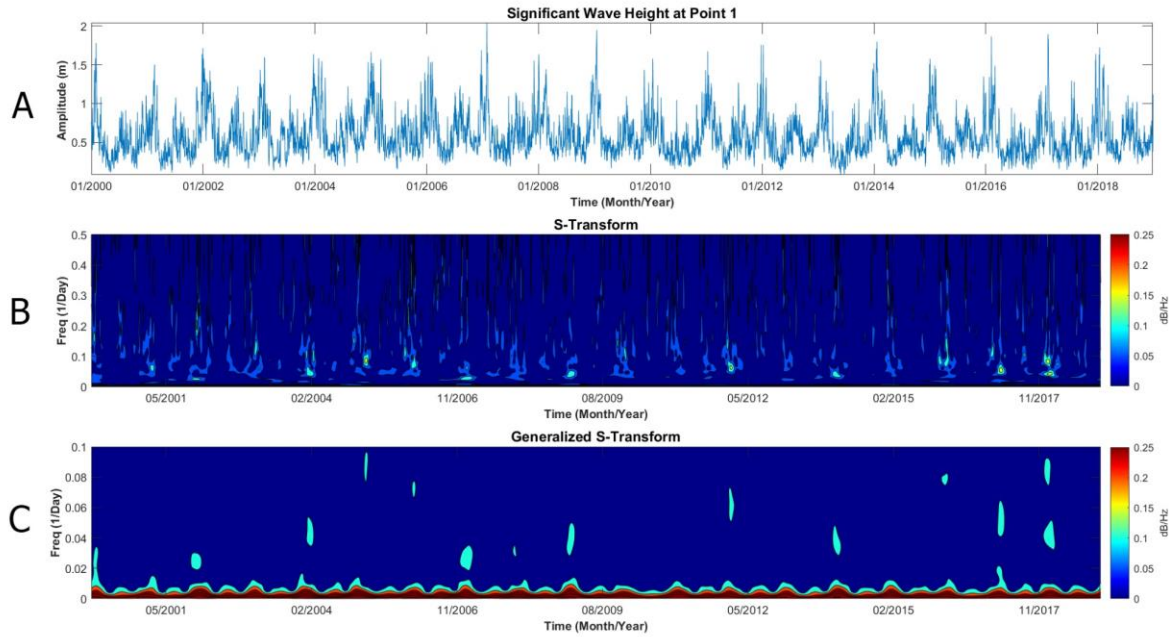

Figure 5. Time series data (A), S-Transform analysis (B) dan GST (C) analysis of SWH at the first point.

S-Transform and GST analysis were also carried out for significant wave height data as shown in Figure 5. Figure 5A shows daily data for SWH from 2000-2018 with the x-axis representing time and the y-axis representing SWH (m). Figure 5B shows a peak frequency that tends to be found in the middle of every year especially around June to July. Peak frequency value is 0.1/day - 0.3/day (3 - 10 days period). It is also seen that the low frequency is more dominant than the high frequency.

Figure 5C is GST analysis, which peak frequency is 0.01/day - 0.1/day (10 - 90 days period). Thus, significant wave height and wind speed are affected by Monsoon and MJO.

S-Transform and GST results on significant wind speed and wave height for points 2 and point 3 are also strongly influenced by MJO and Monsoon. However, at points 2 and 3 the peak of the monsoon is seen at the beginning of the year (January-February). This difference can be caused by the geographical location and the different topography of the sea surface. So that we get two main components that regulate wind speed and significant wave height variability from year to year. 2000 - 2018 namely MJO and Monsoon.

In general, SWH and wind speed climatological conditions in Indonesia are largely influenced by the monsoon cycle (Habibie and Fitria, 2019). The active period of this monsoon is about 3 months followed by a transition period before switching to the monsoon in the opposite direction. In general, the determination of the season is based on changes in the seasonal direction of this wind (Oliver, 2005). The main characteristic of an active monsoon is the presence of persistent winds, namely winds that have almost the same speed and direction in the territory of Indonesia. The longer the area is crossed by this persistent wind (fetch), the higher the wave that will be formed (Habibie and Fitria, 2019). It can also be seen that the high intensity shown in green occurs around the beginning of the year (January – February), where at that time the west season is occurring, and another high intensity is during the east season which occurs around July – August. Low intensity occurs during the transition season.

Frequency Domain Filtering Analysis

EMD, S-Transform, and GST analysis found Monsoon and MJO strongly affect SWH and wind speed variability. A filtering process will be carried out which aims to see the effect of the phenomenon so that it can be seen the magnitude of the

effect of the signal of the phenomenon on the total significant wave height and wind speed variation.

The bandpass filter process is carried out to see the effect of MJO and Monsoon signals on SWH and wind speed at three observation points. The cutoff period is 15 - 90 days for the MJO effect and 11-13 months for the Monsoon effect. Figure 6A shows the overlay of total SWH (yellow line), SWH affected by MJO (red line), and SWH affected by MJO + Monsoon (black line) at Point 1. The SWH time series pattern of MJO influence corresponds to and follows the total SWH pattern. Thus, MJO has the greatest influence on the total SWH variation. SWH affected by MJO + Monsoon is getting closer to the total SWH value. Figure 6B shows the residual value marked by blue lines which fluctuated with an average residual absolut is 0.0966m. This indicates that other factors affect the total SWH value with a small effect.

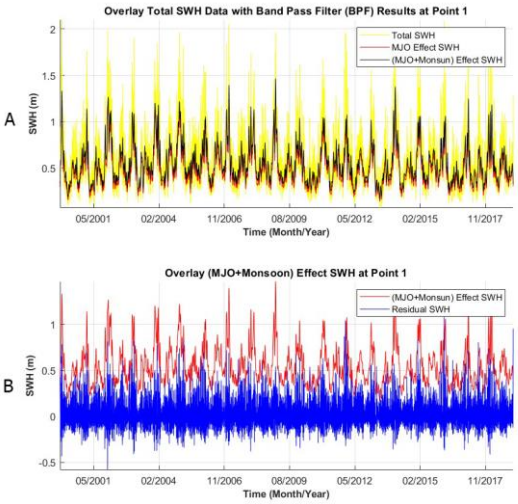

Figure 6. SWH filtering results due to the influence of MJO and Monsoon (A) and residual SWH (B) at the first point.

The Scatter plot between the total SWH data and the MJO and Monsoon effect SWH is shown in Figure 7. Two data are interconnected and have a linear correlation. A linear relationship is shown in the correlation coefficient and RMSE value which are shown in Table 1. The correlation coefficient SWH affected by MJO and Monsoon with total SWH are 0.8866 and 0.6494 and RMSE values are 0.1513m and 0.5763m, respectively. The SWH value of the MJO + Monsoon effect produces a smaller RMSE value of 0.1330m and the gradient value is 0.8. Thus, the total SWH value at point 1 is dominantly influenced by MJO and Monsoon up to 80% of the total SWH.

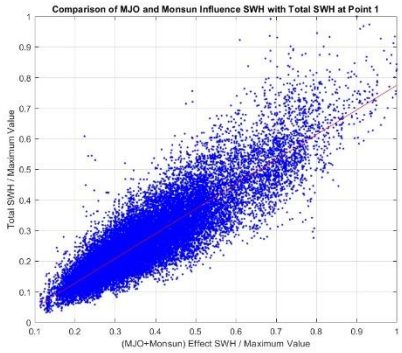

Figure 7. Scatter plot diagram of SWH total and SWH influence (MJO + Monsoon) at the first point.

Frequency domain filtering analysis was carried out on SWH and wind speed at points 1, 2, and 3. Correlation coefficients and RMSE values at each observation point are shown in Table 1. SWH and wind speed values at points 1, 2, and 3 are dominantly influenced by MJO and Monsoon with an average gradient value of 72%.

Table 1. Correlation and RMSE linear regression on the value of SWH and Wind Speed

Variable	Correlation coefficient		RMSE			Gradient (MJO + Monsoon) / total
	MJO	Monsoon	MJO	Monsoon	MJO + Monsoon	
SWH - 1	0.8866	0.6494	0.1513m	0.5763m	0.1330m	0.8090
SWH - 2	0.9038	0.6874	0.2654m	0.9586m	0.2377m	0.7259
SWH - 2	0.8038	0.4025	0.1321m	0.4625m	0.1188m	0.6406
V -1	0.7892	0.5552	1.3004m/s	4.1261m/s	1.1958m/s	0.8017
V - 2	0.5780	0.3025	1.4806m/s	3.2802m/s	1.4302m/s	0.5954
V - 3	0.8015	0.5446	1.4985m/s	4.7172m/s	1.3814m/s	0.7926

***Wind Speed Spatial Interpolation in* 2017**

Figure 8 is a spatial interpolation of wind speed analysis at a height of 10 m using the ordinary kriging method with spatial analysis tools found in ArcGIS software using a semi-spherical variogram model. Figure 8 shows spatial interpolation of the daily average wind speed from January to December 2017. Every month it is seen that large wind speeds are generally dominated in the south of the Natuna Sea. In general, the waters of Natuna Island are controlled by a monsoon wind system that changes its direction according to the seasons (Wyrtki, 1961; Anggara *et al.*, 2018; Muliati *et al.*, 2019).

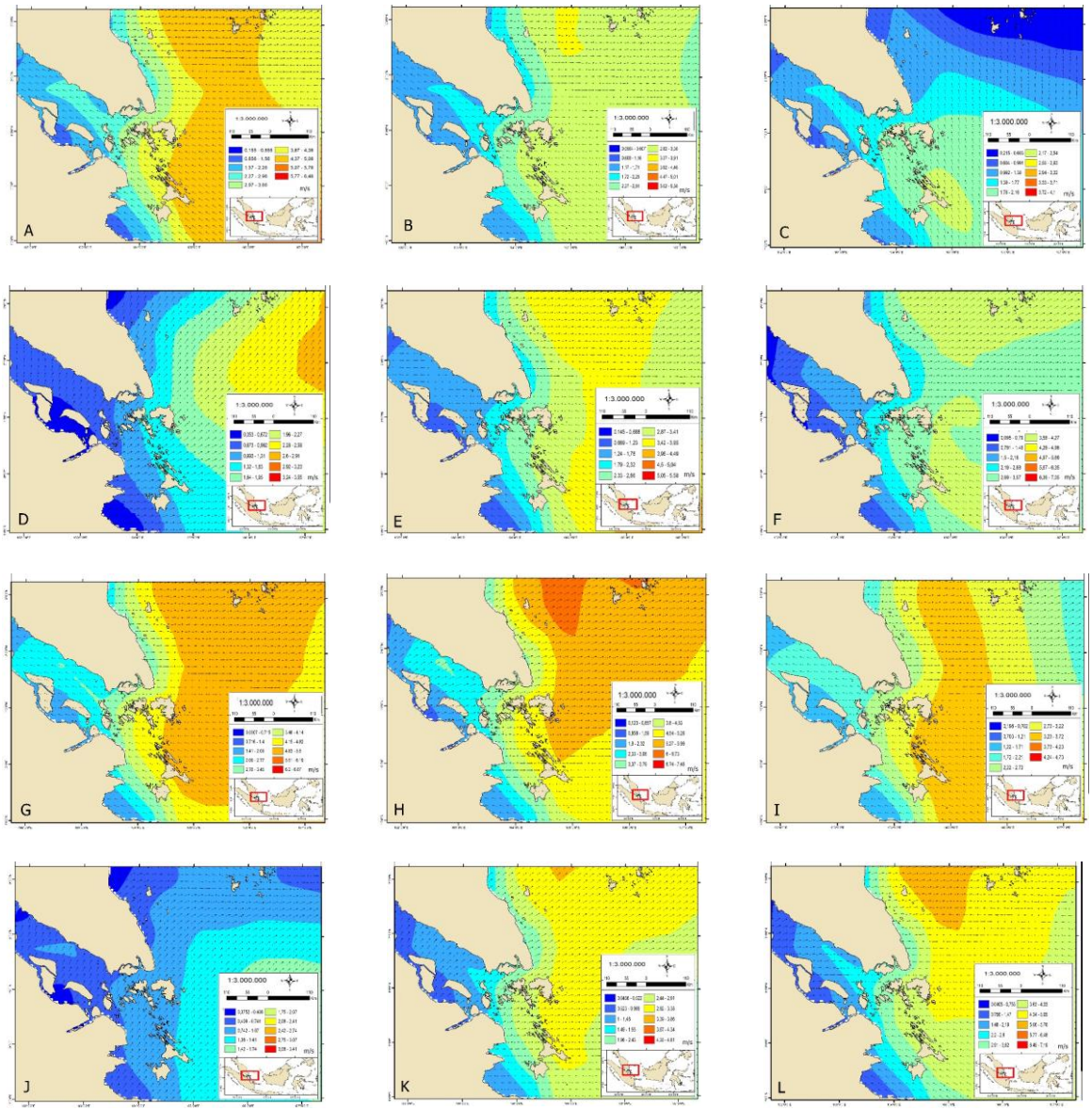

Figure 8. Spatial interpolation of 2017 average daily wind speed around ALKI-1 in January (A), February (B), March (C), April (D), May (E), June (F), July (G), August (H), September (I), October (J), November (K), and December (L).

The west monsoon that occurred in January and February (Figure 8A and 8B) in Natuna waters showed that the wind speed was dominantly blowing from the north, the highest with a value of 5 m/s. The characteristic wind speed in the west monsoon reaches its peak in January. The orbit of the sun causes the circulation of monsoon winds that come from high-pressure areas in the subtropical northern

latitudes to low-pressure areas in the subtropical southern latitudes (Wyrtki, 1961).

The first transitional season winds occurred in March, April, and May (Figure 8C, 8D, and 8E) seen that the wind direction is dominated by the wind from the northeast, there is a shift in the dominant direction of the wind. The movement of the sun from the south latitude (tropic of Capricorn) to the north latitude (tropic of Cancer) causes a transition to changes in wind speed and direction (Wyrtki, 1961; Afriady *et a*l., 2019).

There is a change in monsoon wind circulation from the west monsoon and transition 1. East monsoon occurred in June, July, and August (Figure 8F, 8G, and 8H) where there is a reversal of wind direction as shown in Figure 8C, 8D, and 8E. Direction dominant wind coming from the south with speeds up to 4m/s.

Second transitional season winds occurred in September, October, and November (Figure 8I, 8J, and 8K). Waters of the Natuna Sea, show that the wind direction is dominated by winds from the southwest with a speed of up to 3.5 m/s. The influence of the movement of the sun from the north latitude (tropic of Cancer) to the south latitude (tropic of Capricorn) occurs in September, October, and November (Figure 8I, 8J, and 8K) (Wyrtki, 1961; Afriady *et al*., 2019) causes the transition of changes in wind direction.

Wind speed in the waters of the Riau Islands is relatively lower than the waters of the Natuna Sea. West season (Figure 8A and 8B) show dominant winds coming from northwest to north with wind speeds of up to 4 m/s. The first transitional season (Figure 8C, 8D, and 8E) shows wind speed change varying with average wind speeds ranging from 2m/s – 3.5 m/s. The wind pattern varies due to the first transitional season being between the west and east seasons. The wind blows are still influenced by the two seasons and the position of the sun is around the equator, so the temperature difference between the Asian continent and the Australian continent is small.

East monsoon (Figure 8F, 8G, and 8F) show dominant winds occur coming from the southeast with the distribution of wind speed values tending to be almost the same, except near the island of Bangka. Wind speed values ranged from 2 - 3.5 m/s. The second transitional season (Figure 8I, 8J, and 8K) shows the value of the average range wind speed from 2m/s - 3 m/s. The second transitional season shows dominant wind direction occurs from the southeast to the southwest.

SWH Spatial Interpolation in 2017

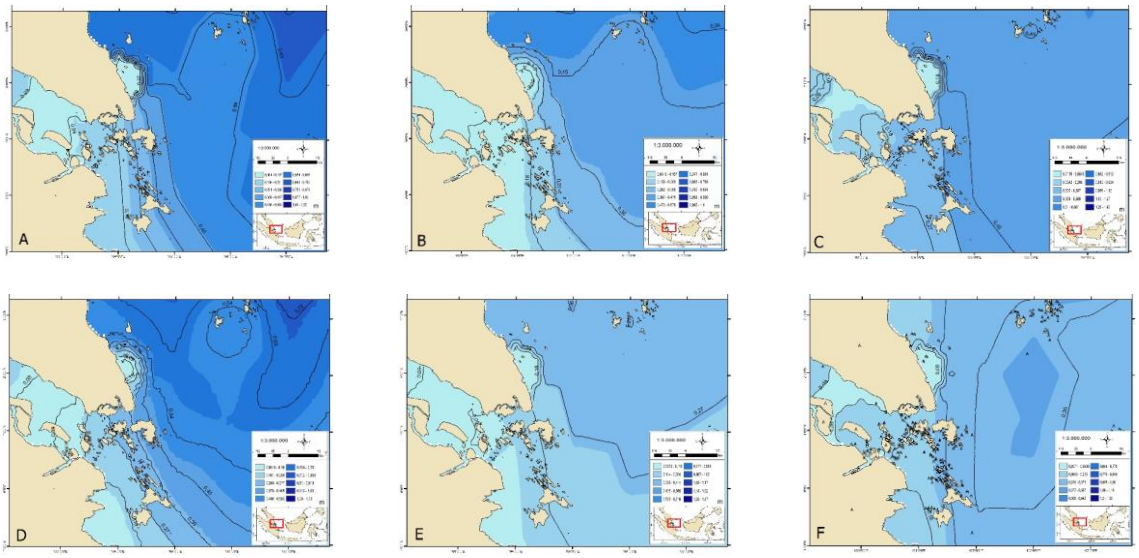

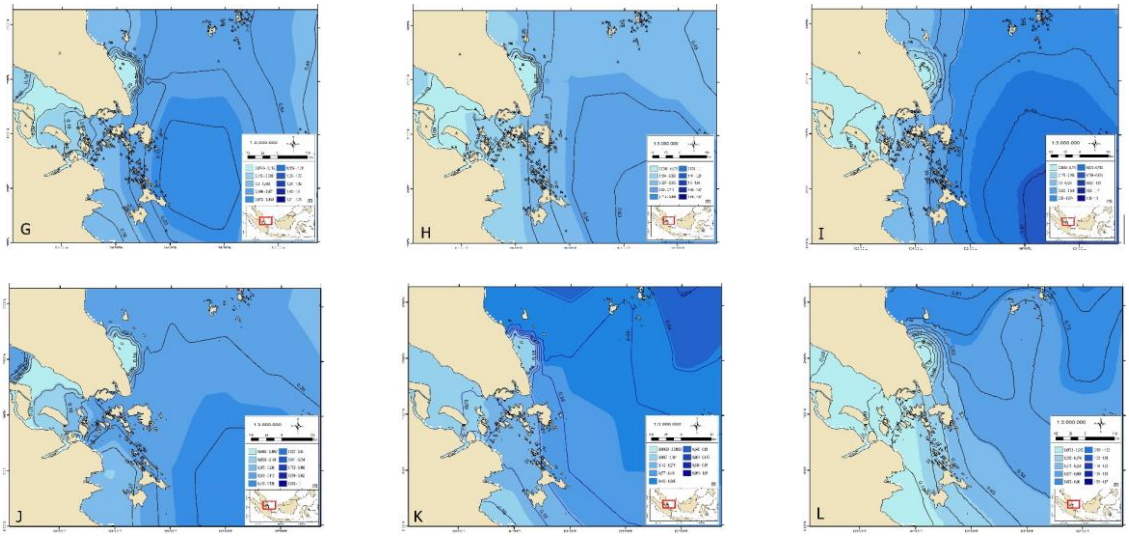

Figure 9. The spatial interpolation of the 2017 significant monthly mean wave heights around ALKI-1 in January (A), February (B), March (C), April (D), May (E), June (F), July (G), August (H), September (I), October (J), November (K), and December (L).

Figure 9 shows spatial interpolation of the 2017 significant wave height analysis from January to December. Every month it is seen that the height of significant waves is generally dominated in the south of the Natuna Sea. The results of this study complement the research on the characteristics of ocean waves previously conducted by Muliati *et al.* (2018), Anggara *et al*. (2019), and Afriady *et al*. (2019).

West Season (Figure 9A and 9B) show the direction SWH occurs from northwest to north and ranges value SWH from 0.8 to 1.5 m. This season, the SWH value is highest than in other seasons. This is caused by the factor of the length of the wind blowing (wind duration), the magnitude of the duration of the wind is due to the northern area of the Karimata Strait directly adjacent to the South China Sea and the Pacific Ocean (Jumarang, 2015).

The first transitional season (Figure 9C, 9D, and 9E) shows a range value SWH from 0.5 to 0.75 m. SWH is significantly the lowest than other seasons. This is influenced by the dominant wind direction that occurs varies and the duration of the wind is shortest than in other seasons (Jumarang, 2015).

East monsoon (Figure 9F, 9G, and 9H) generally occurs in the direction of the waves from the southeast. The distribution of SWH tends to be almost the same strength. except near the waters of the Riau Islands due to approaching coastal areas. SWH is significantly higher in this season than first and second transitional seasons. This is caused by the factor of the length of time the wind blows from the dominant wind direction. The long duration of the wind is due to the dominant wind direction from the southeast coming from the Java Sea, so the wind blows no obstacles from the mainland (Wyrtki, 1961, Jumarang, 2015, Muliati et al. (2018), Anggara et al. (2019).

The second transitional season (Figure 9I, 9J, and 9K) shows wave direction occurs from southeast to southwest and range value SWH from 0.5 to 1 m. SWH value in this season is higher than in the first transitional season and lower than in the west and east monsoons. This is due to the shorter duration of the winds than the west and east monsoons, although the difference in wind speed is not that great. so that the minimum fetch formed is shorter (Jumarang, 2015).

Effect of Monsoons on SWH at Observation Points 1, 2, and 3.

Figure 10 is the average SWH at observation points 1, 2, and 3, show points 1 and 2 minimum value SWH in east monsoon (JJA). Observation points 3

shows the maximum value SWH in the second transition monsoon (SON).

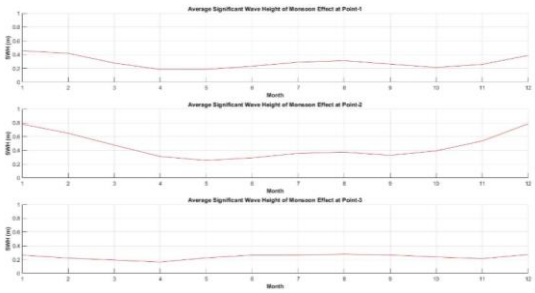

Figure 10. Average monthly significant wave height from 2000-2018 at points 1,2 and 3 due to the influence of the Monsoon.

Points 1 and 2 in the DJF period of maximum significant wave height with the dominant wave direction propagation coming from west to east, then turning southeast when entering the strait and increasing SWH. This should be done by all parties who carry out activities in these waters, especially fishermen and ferry service providers because high waves in these months increase the risk of other months. Overall, the DJF period in January has a longer duration of wind speed and high wind speed.

Point 3 of the maximum SWH formed in the waters of the Malacca Strait generally occurs in the SON period and the minimum in the JJA period. The pattern of wind coming affects the pattern of sea waves formed in the waters of the Malacca Strait. The wind movement in the waters of the east coast of the northern part of the island of Sumatra is more dominant than the north and has the highest average speed so SWH formed in the waters of the east coast of the northern part of the island of Sumatra are more dominant originating from the north. SWH originating from the north are sea waves with higher than average height compared to sea waves that are formed and come from several other wave generation directions. This is inseparable from the influence of wind speed, geographical position, distance, direction, and the initial location of waves in the deep sea. Ocean waves originating from the north coast have a generation distance that is longer than the generation distance from the south, with the wind speed blowing from the north having a higher average speed than the wind blowing from the south. The location of generation SWH is originating from the Singapore Strait to the north of the coast and has a deeper level of water depth than the waters on the southern coast so the SWH formed from the north will be higher than the waves originating from other generation directions.

Effect of MJO on SWH at Observation Points 1, 2, and 3.

The way to detect MJO is to analyze its phase using a Hovmoller diagram. In general, the MJO cycle is divided into 8 phases as shown in Figure 11. The Real-Time Multivariate MJO Index (RMM) is used for MJO monitoring by the Australian Meteorological Agency.

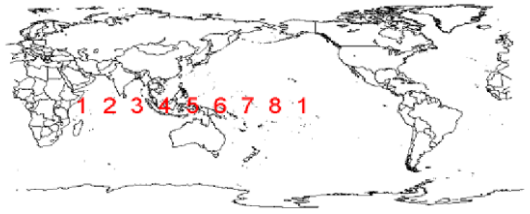

Figure 11. Approximation of the MJO Location based on the RMM Phase Index (Meinke *et al*., 2014)

Figure 12 shows the effect of the MJO of each phase on the SWH. MJO events were analyzed to find the effect of active MJO events in the period 2000-2018 for points 1,2, and 3. The RMM amplitude values for phases 1-8 MJO positively affect wave height. The effect of the largest to the smallest MJO is points 2, 1, and 3 respectively.

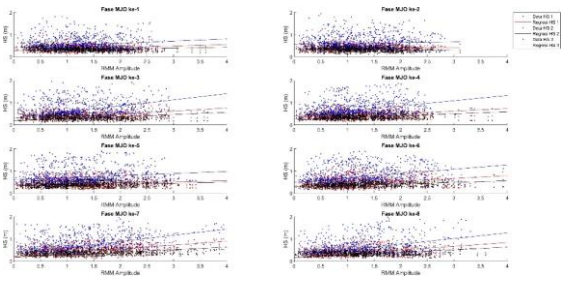

Figure 12. The linear influence of the amplitude of each RMM phase on the value of the wave height is significant.

Points 1, 2, and 3 show the same behavior, when there is an increase in the RMM amplitude in each phase, there is a significant increase in SWH. The slope value of each RMM linear regression to wave height is shown in Table 2 to see the order of influence of the MJO phase on significant wave height and wind speed. It is also the same as wind speed (figure not shown).

Table 2. The slope of the linear regression of the RMM amplitude concerning significant wave height and wind speed in each MJO phase.

MJO Phase	SWH			Wind Wave		
	Point 1	Point 2	Point 3	Point 1	Point 2	Point 3
1	0.0676	0.0969	0.0417	0.458	0.296	0.510
2	0.0010	0.0315	-0.0259	-0.182	-0.073	0.000
3	0.1421	0.2769	0.0977	0.802	0.747	1.179
4	0.1216	0.2345	0.0907	0.764	0.661	1.005
5	0.0416	0.0922	0.0397	0.296	0.211	0.438
6	0.1166	0.1939	0.0705	0.801	0.430	0.883
7	0.1724	0.2794	0.1139	1.183	0.735	1.326
8	0.1678	0.2543	0.1183	1.198	0.755	1.280

The three largest slopes of the linear regression of RMM amplitude on SWH and wind speed occurred in phases 4, 7, and 8. In this phase, the increase in SWH and wind speed significantly affected the increase in RMM amplitude. The three lowest slopes are in phases 1, 2, and 5 MJO. In this phase, the active MJO has no significant effect on the SWH value and speed for points 1, 2, and 3.

The MJO develops and is dominantly seen in the southern Indian Ocean region heading eastward through the Australian territory and up to the western Pacific Ocean with a range of 15ºLN - 15ºLS (Madden & Julian, 1971). MJO activity tends to be stronger in boreal winter (DJF) and tends to be weaker in boreal summer (JJA) (Madden and Julian, 1994). From year to year, the MJO has varied strengths. The MJO phenomenon is related to the formation of hot pools in the eastern Indian Ocean and the western Pacific Ocean so that the movement of the MJO to the east is always followed by thick cumulus convection (Gottschalck *et al*., 2008). So that this result can be used in ship voyages, if there is an active MJO in phases 4, 7, and 8 and during the DJF period, so that it crosses the waters towards the coast.

CONCLUSION

The variability of SWH and wind speed is influenced by atmospheric phenomena from the results of EMD, ST, and GST data analysis. SWH and wind speed are influenced by MJO and monsoon phenomena significantly. SWH and wind speed at points 1 and 2 were greatest in the DJF period, then decreased in the MAM period, and rose again in the SON period, but the increase was not significant so the values obtained were not much different from the JJA period. SWH and wind speed at point 3 are maximum in the SON period and are relatively the same as in other periods. MJO has a positive effect on SWH and wind speed from phases one to eight for points 1, 2, and 3. The 4, 7, and 8 MJO phases affect SWH and wave speed significantly. The 1,2, and 5 MJO phases affect SWH and wind speed weakly.

BIBLIOGRAPHY

Afriady, A., Alam, T.M. and Ismail, M.F.A., 2019. Pemanfaatan Data Angin untuk Karakteristik Gelombang Laut di Perairan Natuna Berdasarkan Data Angin Tahun 2009–2018. *Buletin Oseanografi Marina Inpres*, *8*(2), pp.55-60. https://doi.org/10.14710/buloma.v8i1.25304

Anggara, P.D., Alam, T.M., Adrianto, D. and Pranowo, W.S., 2018, July. The wave characteristics in Natuna Sea

and its adjacent for naval operation base purposes. In *IOP Conference Series: Earth and Environmental Science* (Vol. 176, No. 1, p. 012003). IOP Publishing. https://doi.org/10.1088/1755-1315/176/1/012003

Bahtiyar, A.D.R., Hoyyi, A. and Yasin, H., 2014. Ordinary Kriging Dalam Estimasi Curah Hujan Di Kota Semarang. *Jurnal Gaussian*, *3*(2), pp.151-159. https://doi.org/10.14710/j.gauss.v3i2.5900

Balbeid, N., Atmadipoera, A.S. and Koropitan, A.F., 2015. Response of Sea Surface Temperature (SST) and Chlorophyll-a on Madden Julian Oscillation (MJO) in Indonesian Seas. *Jurnal Ilmu dan Teknologi Kelautan Tropis*, *7*(2). https://doi.org/10.29244/jitkt.v7i2.11035

Fatimah, S., 2019. *Pengantar Transportasi*. Myria Publisher.

Gottschalck, J. and Higgins, W., 2008. Madden Julian oscillation impacts. *NOAA Climate Prediction Center.*

Habibie, M.N. and Fitria, W., 2019. Kajian indeks variabilitas tinggi gelombang signifikan di Indonesia. *Jurnal Segara*, *14*(3), pp.159-168. http://dx.doi.org/10.15578/segara.v14i3.6650

Hadi, S. and Sugianto, D.N., 2012. Model distribusi kecepatan angin untuk peramalan gelombang dengan menggunakan metode Darbyshire dan SMB di perairan Semarang. *Buletin Oseanografi Marina*, *1*(3), pp.25-32. https://doi.org/10.14710/buloma.v1i3.6907

Harris, A., Prakoso, L.Y. and Sianturi, D., 2021. Strategi Pertahanan Laut dalam Rangka Ancaman Keamanan di Alur Laut Kepulauan Indonesia II. *Strategi Pertahanan Laut*, *5*(1). https://doi.org/10.33172/spl.v5i1.648

Huang, C.J., Shen, Y., Chen, Y.H. and Chen, H.C., 2021. A novel hybrid deep neural network model for short-term electricity price forecasting. *International Journal of Energy Research*, *45*(2), pp.2511-2532. https://doi.org/10.1016/j.egyr.2021.04.009

Jones, C., Waliser, D.E. and Gautier, C., 1998. The influence of the Madden–Julian oscillation on ocean surface heat fluxes and sea surface temperature. *Journal of Climate*, *11*(5), pp.1057-1072. https://doi.org/10.1175/1520-0442(1998)011<1057:TIOTMJ>2.0.CO;2

Juan, N.P. and Valdecantos, V.N., 2022. Review of the application of Artificial Neural Networks in ocean engineering. *Ocean Engineering*, *259*, p.111947. https://doi.org/10.1016/j.oceaneng.2022.111947

Jumarang, M.I.,2015, Studi Variabilitas Tinggi dan Periode Gelombang Laut Signifikan di Selat Karimata. *POSITRON*, *5*(1). https://doi.org/10.26418/POSITRON.V5I1.9737

Khetarpal, P. and Tripathi, M.M., 2020. A critical and comprehensive review on power quality disturbance detection and classification. *Sustainable Computing: Informatics and Systems*, *28*, p.100417. https://doi.org/10.3390/s21113910

Kolawole, E.S., Ali, W.H., Cofie, P., Fuller, J., Tolliver, C. and Obiomon, P., 2015. Design and Implementation of low-pass, high-pass and band-pass finite impulse response (FIR) filters using FPGA. *Circuits and Systems*, *6*(02), p.30. http://dx.doi.org/10.4236/cs.2015.62004?

Kurniawan, R. and Khotimah, M.K., 2016. Ocean wave characteristics in Indonesian Waters for sea transportation safety and planning. *IPTEK The Journal for Technology and Science*, *26*(1). http://dx.doi.org/10.12962/j20882033.v26i1.767

Kusumastanto, T., 2021. 7.9 Arah Kebijakan dan Strategi Pembangunan Indonesia sebagai Negara Maritim. *Pengembangan Perikanan, Kelautan, dan Maritim*

untuk Kesejahteraan Rakyat Volume II, p.741.

Listiyono, Y., Prakoso, L.Y. and Sianturi, D., 2021. Strategi Pertahanan Laut dalam Pengamanan Alur Laut Kepulauan Indonesia untuk Mewujudkan Keamanan Maritim dan Mempertahankan Kedaulatan Indonesia. *Strategi Pertahanan Laut*, *5*(3). https://doi.org/10.33172/spl.v5i3.642

Lokhande, S.F., Oling, G.W. and Pedraza, J.F., 2017. Linear response of entanglement entropy from holography. *Journal of High Energy Physics*, *2017*(10), pp.1-40. https://doi.org/10.1007/JHEP10(2017)104

Madden, R.A. and Julian, P.R., 1971. Detection of a 40–50 day oscillation in the zonal wind in the tropical Pacific. *Journal of Atmospheric Sciences*, *28*(5), pp.702-708. https://doi.org/10.1175/1520-0469(1971)028<0702:DOADOI>2.0.CO;2

Madden, R.A. and Julian, P.R., 1972. Description of global-scale circulation cells in the tropics with a 40–50 day period. *Journal of Atmospheric Sciences*, *29*(6), pp.1109-1123. https://doi.org/10.1175/1520-0469(1972)029<1109:DOGSCC>2.0.CO;2

Madden, R.A. and Julian, P.R., 1994. Observations of the 40–50-day tropical oscillation - A review. *Monthly weather review*, *122*(5), pp.814-837. http://dx.doi.org/10.1175/1520-0493(1994)122<0814:OOTDTO>2.0.CO;2

Marelsa, N.F. and Oktaviandra, Y., 2019. Analisis Karakteristik Gelombang Laut Menggunakan Software Windwave-12 (Studi Kasus: Kepulauan Mentawai). *OSEANA*, *44*(2), pp.10-24. https://doi.org/10.14203/oseana.2019.Vol.44No.2.23

Muliati, Y., Tawekal, R.L., Wurjanto, A., Kelvin, J. And Pranowo, W.S., 2019. Wind Wave Modeling In Natuna Sea: A Comparison Among SWAN, SEAFINE, And Era-Interim. *Geomate Journal*, *16*(54), Pp.176-184. https://geomatejournal.com/geomate/article/view/2666

Oliver, J.E., 2005. Encyclopedia of World Climatology. Berlin, Heidelberg, New York: Springer Science & Business Media. https://doi.org/10.21660/2019.54.93272

Rozi, M.T.A., Ariani, B. and Wahyudi, D., 2021. Analisis numerik pengaruh kecepatan terhadap seakeeping kapal patroli pada daerah pelayaran sea state 7. *ALE Proceeding*, *4*, pp.13-17. https://doi.org/10.30598/ale.4.2021.13-17

Sahoo, S.K., Katlamudi, M., Barman, C. and Lakshmi, G.U., 2020. Identification of earthquake precursors in soil radon-222 data of Kutch, Gujarat, India using empirical mode decomposition based Hilbert Huang Transform. *Journal of Environmental Radioactivity*, *222*, p.106353. https://doi.org/10.1016/j.jenvrad.2020.106353

Saputra, S., Ngii, E., Chaerul, M., Suseno, D.N., Sinambela, M., Suseno, D.A.N., Saad, M., Yesica, R. and Devianto, L.A., 2020. *Pengelolaan Wilayah Pesisir yang Terpadu untuk Ketahanan Nasional*. Yayasan Kita Menulis.

Siregar, D.C., Ardah, V.P. and Navitri, A.M., 2019. Analisis Kondisi Atmosfer Terkait Siklon Tropis Pabuk serta Pengaruhnya terhadap Tinggi Gelombang di perairan Kepulauan Riau. *Tunas Geografi*, *8*(2), pp.111-122. https://doi.org/10.56064/jps.v24i1.676

Syafril, K.S. dan Sujarwanto, S., 2015. Pengembangan Pelayaran Perintis pada Perintis Pulau-Pulau Terisolir di Kepulauan Riau. *Jurnal Penelitian Transportasi Laut*, *17*(2), pp.43-53. https://doi.org/10.25104/transla.v17i2.1411

Usman, F., Tinungki, G.M. and Herdiani, E.T., 2022. Model Semivariogram dalam Menaksir Sebaran Kadar Ni Menggunakan Metode Ordinary Kriging (Studi Kasus Endapan Nikel

Laterit di PT Vale Indonesia Tbk). *SPECTA Journal of Technology*, *6*(1), pp.55-67. https://doi.org/10.35718/specta.v6i1.697

Wang, H., Zhang, Y.M. and Mao, J.X., 2022. Sparse Gaussian process regression for multi-step ahead forecasting of wind gusts combining numerical weather predictions and on-site measurements. *Journal of Wind Engineering and Industrial Aerodynamics*, *220*, p.104873. https://doi.org/10.1016/j.jweia.2021.104873

WMO. 2001. *Guide to Wave Analysis and Forecasting*. WMO-no. 702.

Wyrtki, K., 1961. *Physical oceanography of the Southeast Asian waters* (Vol. 2). University of California, Scripps Institution of Oceanography. https://escholarship.org/uc/item/49n9x3t4

Zeiler, A., Faltermeier, R., Tomé, A.M., Keck, I.R., Puntonet, C., Brawanski, A. and Lang, E.W., 2013. Sliding empirical mode decomposition-brain status data analysis and modeling. In *Advances in Intelligent Signal Processing and Data Mining* (pp. 311-349). Springer, Berlin, Heidelberg. https://doi.org/10.1007/978-3-642-28696-4_12